Wetting of the tarsal adhesive fluid controls underwater adhesion in ladybug beetles

Pranav Sudersan,[†] Michael Kappl,[†] Bat-El Pinchasik,[‡] Hans-Jürgen Butt,[†] and Thomas Endlein[*,†]

†*Max Planck Institute for Polymer Research, Ackermannweg 10, 55128 Mainz, Germany*

‡*School of Mechanical Engineering, Tel Aviv University, Tel Aviv-Yafo, Israel*

E-mail: endlein01@mpip-mainz.mpg.de

Abstract

Many insects can climb smooth surfaces using hairy adhesive pads on their legs mediated by tarsal fluid secretions. It was previously shown that a terrestrial beetle can even adhere and walk underwater. The naturally hydrophobic hairs trap an air bubble around the pads, allowing the hairs to make contact to the substrate like in air. However, it remained unclear to what extent such an air bubble is necessary for underwater adhesion. To investigate the role of the bubble, we measured the adhesive forces in individual legs of live but constrained ladybug beetles underwater in the presence and absence of a trapped bubble and compared it with its adhesion in air. Our experiments revealed that on a hydrophobic substrate, even without a bubble, the pads show adhesion comparable to that in air. On a hydrophilic substrate, underwater adhesion is significantly reduced, with or without a trapped bubble. We modelled the adhesion of a hairy pad using capillary forces. Coherent with our experiments, the model demonstrates that the wetting properties of the tarsal fluid alone can determine the ladybugs' adhesion to smooth surfaces in both air and underwater conditions and that an air

bubble is not a prerequisite for their underwater adhesion. The study highlights how such a mediating fluid can serve as a potential strategy to achieve underwater adhesion via capillary forces, which could inspire artificial adhesives for underwater applications.

Keywords

bio-adhesion; capillary force; bubble; insects; gecko

1 Introduction

The question on how insects and other small animals climb smooth and slippery surfaces has fascinated scientists for the past three centuries[1,2]. We know that such animals are able to adhere by using specialised organs on their feet called adhesive pads. These adhesive pads can generally be described as either "smooth" or "hairy". Several insect orders including earwigs, flies, and beetles[3] but also several spiders[4] and arboreal lizards[5] bear hairy pads. Hairy pads show 1) compliance to rough surfaces due to their lower effective modulus, 2) angle dependent adhesion due to asymmetric hair geometry and 3) self-cleaning capability[6], which makes them suitable to adhere to most surfaces reversibly. The hairs themselves (setae) can branch into smaller fibrillar units (spatulae) as seen in spiders and lizards but are typically undivided in most insects. The hairs in many insects can however exhibit different tip geometries, including discoidal, spatula shaped or pointed tips, and distributed throughout the pad depending on sex or species[7]. Single seta force measurements revealed that discoidal shaped seta show larger pull-off forces than spatula shaped or pointed setae[8], illustrating the role of hair geometry in adhesion. Insect tarsal hairs secrete an adhesion-mediating fluid ("wet adhesion") while spiders and geckos rely on their dry hairy pads for attachment ("dry adhesion"). In the "wet adhesion" case, fluid secretion can enforce adhesion through surface tension and viscous forces[9–11], while, "dry adhesion" relies mostly on van der Waals forces[12].

While most of the studies on insect adhesion focused on terrestrial species, underwater insect attachment is much more rare and has been relatively unexplored. Some aquatic insects like diving beetles[13] or midge larva[14] use suction cups to adhere to surfaces. However, underwater adhesion mediated by secreted liquids require the displacement of the water at the interface first and a spreading of the fluid on the substrate. One relatively simple approach is to use an air bubble around the adhesive organs similar to the air bubbles many secondary aquatic insects and spiders carry on their body for breathing underwater[15]. This has been shown in a recent study by Hosoda and Gorb[16] that that female terrestrial green dock beetles *Gastrophysa viridula* can attach quite well to surfaces underwater by using such an air bubble. Their naturally hydrophobic tarsal hairs trap the bubble around the pads when being submerged underwater, which de-wets the surface on contact. It has been hypothesised that a combination of capillary forces due the air bubble and hair secretions within the de-wetted area results in its adhesion underwater. However, it remains unclear if an air bubble is necessary for adhesion and what, if any, contribution it has to the adhesive force. The oily tarsal adhesive fluid found in insects alone might be sufficient in creating the necessary capillary adhesion even without a bubble, given that the fluid remains on the hair tips when submerged. In ladybug beetles, the tip of each seta secretes approximately one femtoliter of tarsal adhesive fluid by each step[17]. The fluid's chemical composition in green dock beetles was identified to be an oil-containing mixture of mostly long chain hydrocarbons[18] with traces of triglycerides, fatty acids and cholesterol in ladybirds *Hemisphaerota cyanea* and *Epilachna vingtipunctuata*[19,20], rendering it immiscible with water.

The goal of this paper is to clarify the current understanding of underwater adhesion seen in terrestrial insects which use hairy pads and secrete an oily fluid for attachment. We used the ladybug beetle (*Coccinella septempunctata*) as an animal model to first experimentally measure adhesion force of its individual pads in air and underwater conditions, both on smooth hydrophilic and hydrophobic glass surfaces. Male ladybug beetles were chosen since they possess adhesive pads having mostly flat discoidal tipped hairs, which allow them to

show superior adhesion on hard surfaces compared to females[21] and they can also walk underwater. Second, we developed a simple theoretical model considering capillary forces to predict the net adhesion force of a hairy pad under different conditions. The case of underwater adhesion was studied both in the presence and absence of a trapped bubble, to decouple the bubble's role in the insect's adhesion. Finally, we discuss key insights gained from our experiments and model with regards to understanding adhesion in other animals. We hope our study to provide new strategies to design bio-inspired materials that show good adhesive properties in both air and underwater conditions, similar to what has been previously reported for terrestrial beetles[16].

2 Experimental

Normal adhesion force measurements on a restrained leg in a live beetle were performed. We focus our study only on a single tarsal adhesive pad of the leg by carefully fixing it (described later) to prevent any dynamic influence of its claws or other tarsomeres/legs, which might otherwise exist under the beetle's natural walking conditions, influencing its adhesion. We characterised adhesion by the pull-off force during detachment, tested on smooth normal and fluorinated glass surfaces representing hydrophilic and hydrophobic substrates respectively. When no water was present, we labelled the mode of contact as "*in air*". Underwater, measurements were done both in the presence and absence of a trapped air bubble ("*underwater: bubble*" and "*underwater: no bubble*", respectively) to investigate the air bubble's role in underwater adhesion. Adhesion force for each of the labelled contact modes were compared for both substrates.

2.1 Material and Methods

2.1.1 Insect preparation

The seven-spotted adult male adult ladybug beetles (*Coccinella septempuctata*) were purchased from Katz Biotech (Baruth, Germany). The beetles were housed in a plastic box filled with leaves, twigs and stones at room temperature and 60-80% relative humidity with daily access to sunlight. They were fed with raisins, honey and water *ad libitum*. The beetles on average weighed 34 ± 4 mg and were experimented on within three weeks of being housed under above conditions.

An individual beetle was first carefully anaesthetised using small amounts of CO_2 sublimating from a piece of dry ice and then glued with a small dollop of epoxy glue on its elytra to the underside of a heavy steel ball. The ball was held in a bracket which allowed free rotational movement of the ball in each direction, thus helping to align the suspended beetle over the substrate (see Fig. 1). The bracket with the ball and the beetle could be further positioned by manual micro-manipulators in all three axes before the experiments. One front left leg was carefully fixed at its tibia to a piece of soft solder wire coming off the steel ball using Blu Tack (Bostik Ltd., U.K.), allowing us to further align the leg to the substrate. Each leg of a male ladybug beetle has two hairy adhesive pads. For the test, we only allowed the distal pad to come into contact with the substrate thus minimising partial or bad contact of the other one. The distal pad was thus restrained by fixing its dorsal side to the wire using Blu Tack. The claws on the leg were also fixed to the wire using epoxy glue to prevent any further wiggling and to prevent the claws from touching the substrate (Fig. 1 top-left inset). Care was taken to ensure the glue doesn't contaminate the rest of the tarsomeres. A small piece of non-sticky Teflon tape helped to keep other legs tucked close to the body and avoided any interference during the adhesion test. After the measurements, the beetle was freed by carefully removing the epoxy glue and Blu Tack without harming it and set free.

2.1.2 Adhesion test

Adhesion measurements were performed on a custom force measurement setup developed in-house (Figure 1). A fibre optic displacement sensor (*Philtec D20, PHILTEC, Inc. USA*) together with a steel bending beam (spring constant = 68.1 N m^{-1}) constituted the vertical force sensor. Beam deflection was calibrated using 4 different known weights to get the corresponding force. A 3D printed substrate holder (22 × 22 × 8 mm) was glued to the end of the bending beam. The holder was designed to enable switching from one substrate to another without removing any glue. It also had transparent side walls which allowed us to fill it with water for the underwater experiments as well as observe the contact. The force sensor was mounted on a stage consisting of a X-piezo element (*Physik Instrumente, Germany*), used for precise lateral movements. Additionally, a separate Z-piezo element, fixed upright, was used for vertical up-down motion, bringing the insect in contact with the substrate from the top. Coarse movements of the bottom stage were done using the XYZ motors (*OWIS GmbH, Germany*). A coaxial illuminated tube microscope (*Navitar, USA*) with 2× objective and a stereo-microscope with 1× objective (*Wild Heerbrugg, Switzerland*) fit with digital video cameras (*Blackfly S, FLIR, USA*, 2448 × 2048 px; *Basler ace U, Germany*, 1280 × 1024 px) were used to record the sample contact with the substrate from ventral and side views respectively. Pad contact area was visualised through the substrate under reflection mode with the help of co-axial illumination. A goniometer was used to adjust the substrate alignment with the ventral view optics to achieve total internal reflection. The data acquisition from the force sensor and cameras, together with the appropriate piezo motion steps were synchronised using a custom LABVIEW (*National Instruments, USA*) program. Force data was acquired at a sample rate of 984 Hz, averaged to 512 points per motion step. Videos were recorded at 20 frames per second.

The vertical and lateral piezos were used simultaneously to perform approach-retract adhesion tests with the substrate to get the pull-off force. However, instead of a simple down-up motion, an additional 100 µm lateral sliding motion in the proximal direction was

introduced after the leg made contact, to ensure most of the hair tips align well with the substrate[7]. A further 10 µm compression step (approach) set all hairs in slight compression which helped further contact with the surface. Next, a short pause (1 s) removed any viscoelastic effects before finally retracting the leg away from the substrate. All approach, retract and lateral slide motion was done at a speed of 62.5 µm s^{-1}. Ventral view video recordings were used for contact area extraction while the side view imaging was used to visually aid orienting the pad with the substrate before a test.

For underwater experiments, 1 ml Milli-Q water was pipetted into the substrate holder (roughly 3 mm water level). The beetle was then partially submerged to allow underwater contact of the pad with the substrate. In order to achieve contact without a trapped air bubble, the water was first degassed separately in a vacuum chamber at 10 mbar pressure for 3 hours and then pipetted into the holder immediately. Before the experiments, the pad was brought into contact with the clean dry surface 10 times repeatedly to ensure the hairs are free of any contaminating particles.

Five force measurements were subsequently performed, each on a fresh spot of the substrate, and averaged for data analysis. Experiments were repeated with five distinct male beetles for each combination of contact mode ("*in air*", ("*underwater: bubble*" and ("*underwater: no bubble*") and substrate chemistry (hydrophilic and hydrophobic). Thus, in total, 30 distinct beetles were tested. After an experiment, the beetle was marked on its elytra and released back into the box to ensure the same beetle was not used for any subsequent adhesion tests.

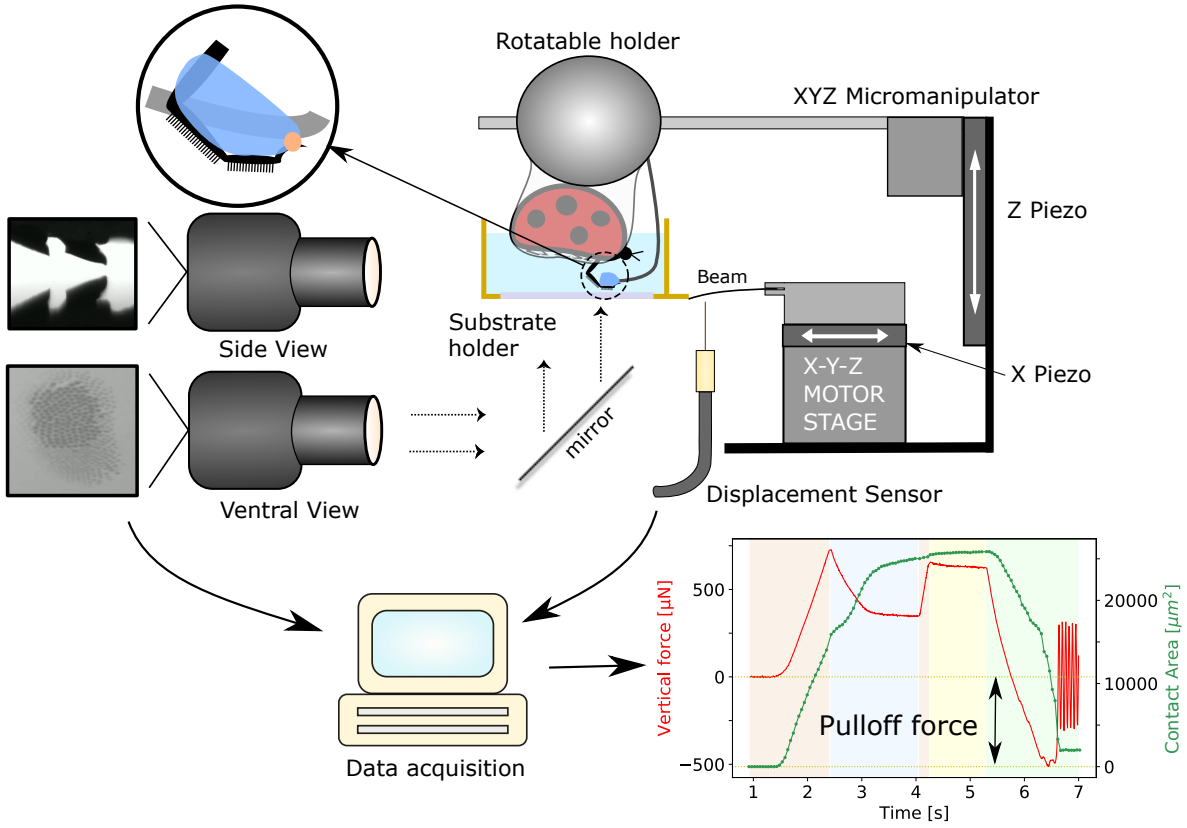

Figure 1: Adhesion test setup (see text for details). Top-left inset shows a magnified cartoon of the beetle's leg constrained to a solder wire (grey) using Blu Tack (blue) and epoxy glue (orange). The recorded force data and contact area of a distal pad are shown in the bottom-right plot, in which, the shaded regions from left to right represent the distinct movement sequence: approach, lateral pull, approach, pause and retract, respectively. Negative force values represent attraction and the minimum force peak during the final retraction step is the adhesion force used for further analysis. An animated version of a typical force recording is available in the Supplementary Material (S2-S4).

2.1.3 Data analysis

Extraction of pull-off force from force data, image processing, plotting and statistical analysis were all performed in "*Buggee*", a software tool written in Python using open-source libraries for synchronous analysis of force data and video recordings (`https://github.com/PranavSudersan/Buggee`).

For measurements in air, the pull-off force was defined as the minimum negative force

during the retraction step (bottom-right plot in Figure 1). For underwater measurements, an additional correction was necessary. When the beetle was partially submerged underwater, its contact line at the water surface shifted, which influenced the force readout due to surface tension and buoyancy. This effect needed to be cancelled. So, a "background" force data was recorded, where the submerged beetle makes no contact with the substrate. This background data was then subtracted from a typical force data with substrate contact to correct for the external surface tension effects. The pull-off force was subsequently calculated from the minima as before.

Data sets were compared for statistical differences using pairwise Student t-test and their corresponding p-value and Common Language Effect Size (CLES) are reported. Shapiro-Wilk test was done for each data set to verify a normal distribution of its residuals and Levene's test was done to check for variance homogeneity, to validate the t-test assumptions. Bonferroni's correction was used to account for multiple comparison between groups.

2.1.4 Substrate preparation

Standard 20 mm wide glass cover-slips were used as the hydrophilic substrate. Glass was wiped with isopropanol, rinsed in water and dried under nitrogen flow before use. For the hydrophobic substrate, the glass cover slip was coated with a fluorosilane via chemical vapour deposition (CVD). First, the glass was cleaned using IPA. The surface was then plasma cleaned in an oxygen plasma chamber (*Femto, Diener Electronic GmbH, Germany*) for 10 min at 120 W. Next, 0.2 ml of Trichloro(1H,1H,2H,2H-perfluorooctyl) silane (PFOTS), procured from Sigma Aldrich, was put in a sealed chamber along with the the cleaned glass. The chamber was placed under 100 mbar pressure for 10 min for the CVD process. Finally, the substrate was annealed at 150℃ for 3 hours. Henceforth, we refer to the hydrophilic normal glass substrate as simply *Glass* and the hydrophobic fluorinated glass substrate as *PFOTS*.

The surface chemistry was characterised by dynamic contact angle measurements, per-

formed with a contact angle goniometer (*OCA 35, DataPhysics Instruments GmbH, Germany*) The substrate's wetting towards a polar (Milli-Q water) and a non-polar (n-hexadecane) liquid was tested. Advancing and receding contact angles were measured for a maximum drop volume of 10 µl and with 0.5 µl s^{-1} flow rate (Table 1).

Table 1: Dynamic contact angles (Mean ± SD, n = 3) of Milli-Q water and n-hexadecane on the different test substrates.

Substrate	Liquid	θ_A	θ_R
Glass	Water	63±5°	20±2°
	n-Hexadecane	<10°	<10°
PFOTS	Water	122±1°	93±2°
	n-Hexadecane	88±2°	56±5°

2.2 Results

In air, adhesion forces of the distal pad of ladybug beetle against glass and PFOTS were similar, i.e. no significant differences were detected (Figure 2 and Table S1.1). In contrast, the underwater adhesion on a PFOTS surface was significantly larger than on glass ($p < 0.001$). This stronger adhesion on PFOTS was observed both in the presence and absence of a trapped bubble. In both cases, the adhesion force reached similar values as in air. In contrast, on glass, adhesion underwater was significantly reduced when compared to dry conditions, irrespective of the presence of a trapped bubble ($p \leq 0.002$). In the presence of a bubble, underwater adhesion on glass was slightly higher (CLES = 0.84, $p = 0.07$).

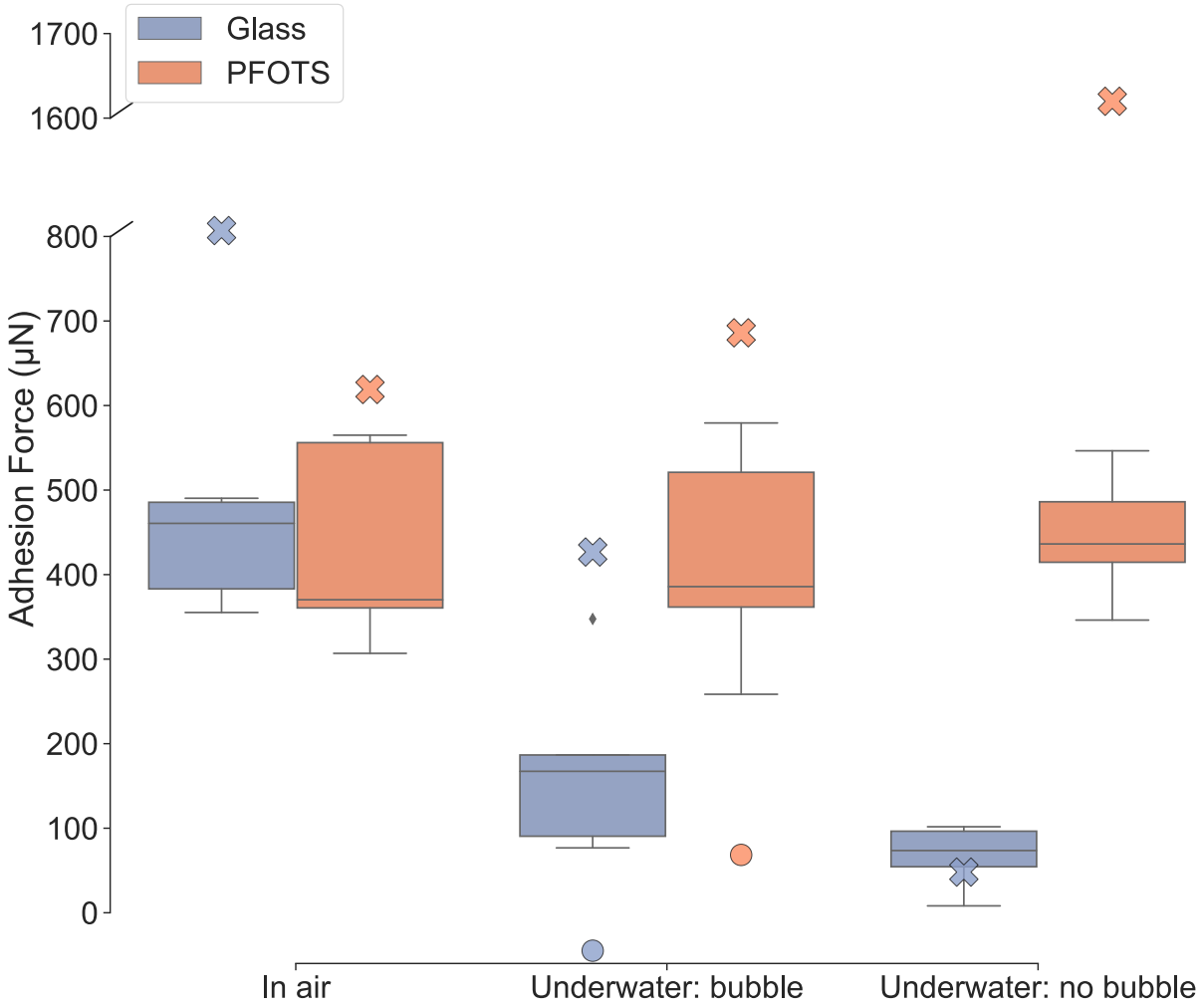

Figure 2: Box-and-whisker plot showing adhesion force measurements of ladybug beetle's (*Coccinella septempuctata*) distal pad on normal hydrophilic glass (blue) and hydrophobic PFOTS coated glass (red) substrates in air and underwater conditions (n=30). The two modes of contact during underwater experiments are represented separately: "*bubble*" and "*no bubble*". Crosses represent theoretical predictions (see text) of adhesion force, while, circles represent the contribution of the bubble itself, calculated from the capillary bridge model. In the model, hair diameter = 4 µm, pad diameter = 200 µm, hair length = 40 µm, N_{hairs} = 500, V_{fluid} = 4.2 fL and V_{bubble} = 1.2 nL. Interfacial tension of the tarsal adhesive fluid in air and water were assumed to be 24 mN m^{-1} and 48 mN m^{-1} respectively and water surface tension is 72 mN m^{-1}.

Apart from the three depicted contact modes, we observed an additional fourth mode which occurred in roughly 25% of our underwater experiments using degassed water. In this scenario, the ventral view recordings show that none of the hairs appear to contact well with either glass or PFOTS substrate (supplementary video S5), unlike the other three contact

modes (supplementary video S2-S4). This "bad contact" scenario only happened underwater and shows no adhesion with either glass or PFOTS substrate. While it was not completely clear why such a contact occurs, there can be two possible reasons. First, the hairs could get bundled due to a small air meniscus within the hairs, resulting in their disorientation. Second, a thin water layer at the substrate interface might not be drained out to allow the hairs to make contact with the substrate, resulting in a loss of adhesion.

3 Theory

3.1 Capillary Bridge Model

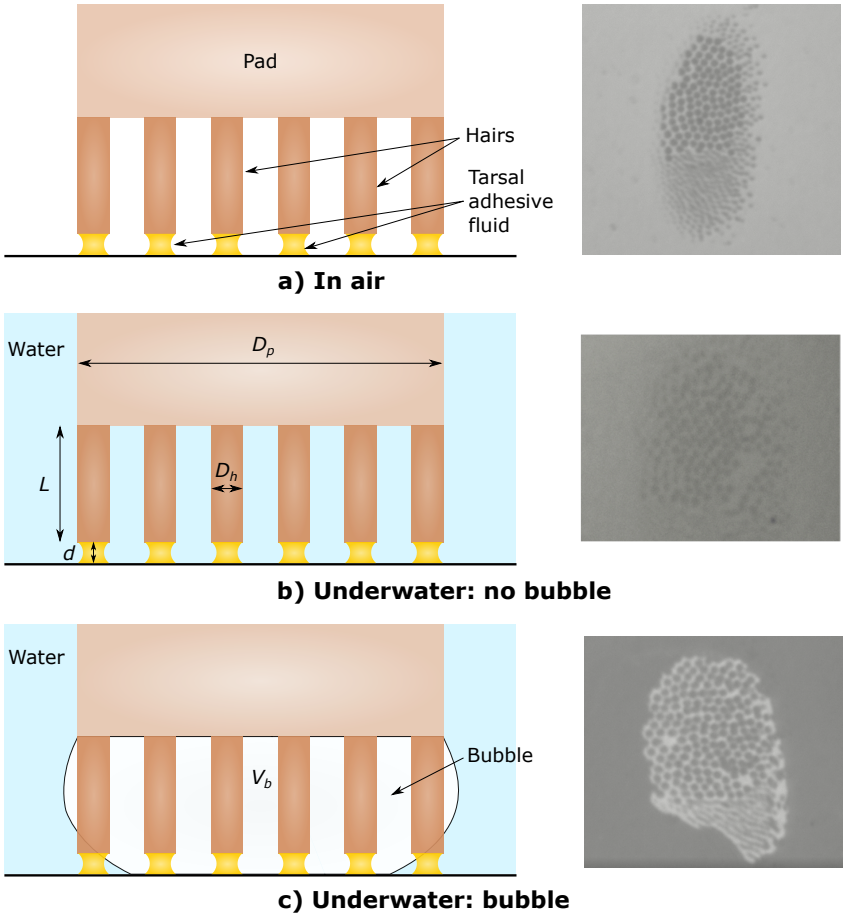

Figure 3: The capillary bridge model of a hairy adhesive pad. The hairs make contact with the substrate (hydrophilic or hydrophobic) in three modes: a) *In air*, where the tarsal adhesive fluid bridges are surrounded by air; b) *Underwater: no bubble*, where the fluid bridges are fully surrounded by water; c) *Underwater: bubble*, where part of the fluid bridges are inside the bubble while others are outside in water (see text for details). The corresponding ventral view contact images of the beetle's pad seen during adhesion experiments are shown on the right.

We modelled the hairy pad as an array of N cylindrical rods of length, L, and diameter, D_h, fixed to a flat circular pad of diameter, D_p (Figure 3). The hairs and the pad were assumed to be perfectly rigid, for simplicity. The tip of each hair has a tarsal adhesive fluid of volume,

V_f, mediating contact with the substrate. The fluid is pinned to the circumference of the hair and forms a capillary bridge of height, d. Similar to our experiments, we considered three modes of contact for the pad: 1) *In air*, 2) *Underwater: no bubble* and 3) *Underwater: bubble*. In the third case, a bubble of volume, V_b, is trapped between the hairs and pinned to the pad circumference.

To characterise the tarsal adhesive fluid and bubble volume, we defined two radii, s_f and s_b, respectively, by $V_f = \frac{4}{3}\pi s_f^3$ and $V_b = \frac{4}{3}\pi s_b^3$. Here, s_f and s_b are the radii of spheres with equivalent volumes. Fluid and bubble radii were assumed to scale proportional to their corresponding pinned contact diameter. We thus defined the size parameters, $\phi_f = D_h/(2s_f)$ and $\phi_b = D_p/(2s_b)$ for the fluid and bubble respectively, to conveniently scale their volumes relative to the hair and pad diameters they are pinned to.

The net force for cases 1 and 2 can be calculated as:

$$F_{net} = Nf \tag{1}$$

Here, f is the capillary force of a single fluid bridge at a distance, d, in air (f_{air}) or underwater (f_{water}).

For case 3, the net force is given by:

$$F_{net} = N_{in}f_{air} + N_{out}f_{water} + f_{bubble} \tag{2}$$

Here, N_{in} and N_{out} are the number of hairs inside and outside the bubble, respectively, f_{air} and f_{water} are the capillary forces of the fluid bridge inside and outside the bubble, respectively, and f_{bubble} is the capillary force contribution due to the bubble meniscus alone at distance $d + L$.

The capillary force, f, is the sum of two contributions: surface tension and Laplace pressure (equation S1.1). Force versus distance for a single capillary bridge was calculated by Surface Evolver simulations[22] (described in supplementary section S1.1), and used to

obtain F_{net} as a function of d for each mode of contact. The adhesion force of the complete hairy pad system was then obtained from the minima of F_{net}, where negative force values represent attraction.

We considered f_{air} and f_{water} to be distinct terms because the capillary force by the tarsal adhesive fluid would be different in air and underwater due to its different contact angle and interfacial tension in each case. Using the Young-Duprè equations for each case of fluid-air, fluid-water and water-air interface, one can derive the following relation for the contact angle of the tarsal adhesive fluid underwater:

$$\cos\theta_{fw} = \frac{\gamma_{fa}\cos\theta_{fa} - \gamma_{wa}\cos\theta_{wa}}{\gamma_{fw}} \tag{3}$$

Here, θ_{fw} and θ_{fa} are the contact angles of the tarsal adhesive fluid with the substrate in water and air respectively, θ_{wa} is the contact angle of water with the substrate in air, γ_{fa} is the surface tension of the tarsal adhesive fluid, γ_{wa} is the surface tension of water and γ_{fw} is the interfacial tension of the tarsal adhesive fluid with water.

All lengths (D_h, D_p, L, d) were normalised w.r.t. s_f and forces were normalized w.r.t. $\gamma_{fa}s_f$. Interfacial tension values were fixed relative to γ_{fa}. Non dimensional bubble volume was expressed as, $\hat{V_b} = V_b/s_f^3$

Geometric parameters and interfacial properties were kept fixed for all model calculations (Table 2). Here, we assumed the tarsal adhesive fluid to be an oil-like substance and thus the interfacial tension ratios γ_{wa}/γ_{fa} and γ_{fw}/γ_{fa} were assumed to correspond to typical values for oil and water. We considered representative hydrophilic and hydrophobic substrates with θ_{fa} and θ_{wa} values corresponding to a typical glass and fluorinated surface, respectively. The contact area fraction of the hairs relative to the pad, $\alpha = ND_h^2/D_p^2$, hair aspect ratio, L/D_h, and fluid size parameter, ϕ_f, were fixed to values typical for a ladybug's hairy pad.

First, we calculated force-distance curves for a single pinned liquid capillary bridge. Second, the effect of substrate on the force-distance curves of the hairy pad system was compared for each mode of contact. Third, we looked at the effect of changing the bubble volume, $\hat{V_b}$,

on the net underwater adhesion. Finally, the influence of varying the hair diameter, D_h, on adhesion was studied for each case.

Table 2: Fixed parameter values corresponding to the pad's geometry, tarsal fluid and substrate wetting properties used in the capillary bridge model

Property	Value
Contact area fraction, α	0.1
Hair aspect ratio, L/D_h	10
Water surface tension ratio, γ_{wa}/γ_{fa}	3
Tarsal fluid-water interfacial tension ratio, γ_{fw}/γ_{fa}	2
Tarsal fluid size parameter, ϕ_f	2
Hydrophilic substrate	$\theta_{fa} = 6°$, $\theta_{wa} = 24°$
Hydrophobic substrate	$\theta_{fa} = 50°$, $\theta_{wa} = 120°$

3.2 Capillary force of a single liquid bridge

Forces due to a single pinned capillary liquid bridge in contact with a substrate were obtained via Surface Evolver simulations (Figure 4). We see that, generally, the shape of the liquid meniscus determines the strength of its adhesion force. High adhesion is seen for contact angles less than $\sim 70°$ due to a net negative (convex) curvature of the meniscus, while low adhesion is seen for contact angles greater than $\sim 150°$ due to its net curvature being close to zero. The Laplace pressure contribution to the net adhesion force dominates for contact angles less than 100° (Figure 4b). Interestingly, its contribution to the adhesion force is mostly non-repulsive for contact angles greater than 90°. This is because, the low volume of the liquid and its pinned contact line prevents the meniscus from having a high positive (concave) curvature due to geometric constraints. Only for a contact angle of 150°, the liquid's curvature becomes positive, manifested in its slightly repulsive Laplace contribution. Surface tension makes a significant contribution to the net force only for a small range of contact angles close to 90°. For contact angles greater than 150°, the net adhesion force approaches zero.

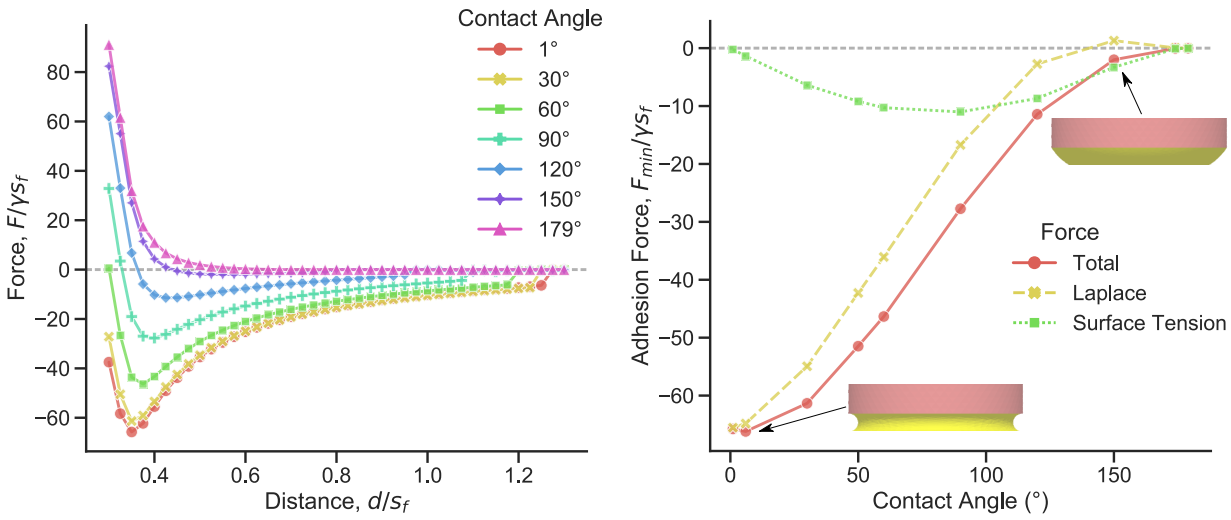

(a) Force-distance curves

(b) Force contributions

Figure 4: Simulation of normalised capillary force of a single liquid bridge in contact with a substrate and pinned to a circular perimeter on top. Fluid size parameter, $\phi_f = 2$. Negative force values represents attraction. a) Force-distance curves are shown for different contact angles of the liquid with the substrate. b) Adhesion forces, calculated from the minima of the corresponding force-distance curves, are plotted as a function of contact angle with the substrate, together with its Laplace and surface tension components (equation S1.1). Simulation snapshots of the liquid meniscus corresponding to angles 6° and 150° are depicted.

The force-distance curves show a general trend of repulsive forces at small distances (Figure 4a). This is a result of the pinned contact line on the top. A limited volume is available for the liquid to occupy when the gap distance is small, causing the meniscus shape to bulge outwards near the pinned contact line. This creates a net positive curvature, resulting in a positive Laplace pressure and thus repulsion. Without pinning, the capillary forces would have shown high attractive forces on a hydrophilic substrate[23].

3.3 Adhesion of a hairy pad: Effect of the substrate

The normalised force-distance curves of a hairy pad system on a hydrophilic and hydrophobic substrate are predicted based on the capillary bridge model and compared for the different contact modes (Figure 5). The forces in each case are calculated from equations (1) and (2) for fixed geometric and interfacial properties (Table 2).

On the hydrophilic substrate ($\theta_{wa} = 24°$), highest adhesion is seen when the hairs contact in air, while lowest adhesion occurs underwater without a trapped bubble. The presence of a bubble leads to intermediate force values. In contrast, on a hydrophobic substrate ($\theta_{wa} = 120°$), highest adhesion is seen for the underwater case without a trapped bubble, much larger than in air. When a bubble is present, the forces are only slightly larger than in air.

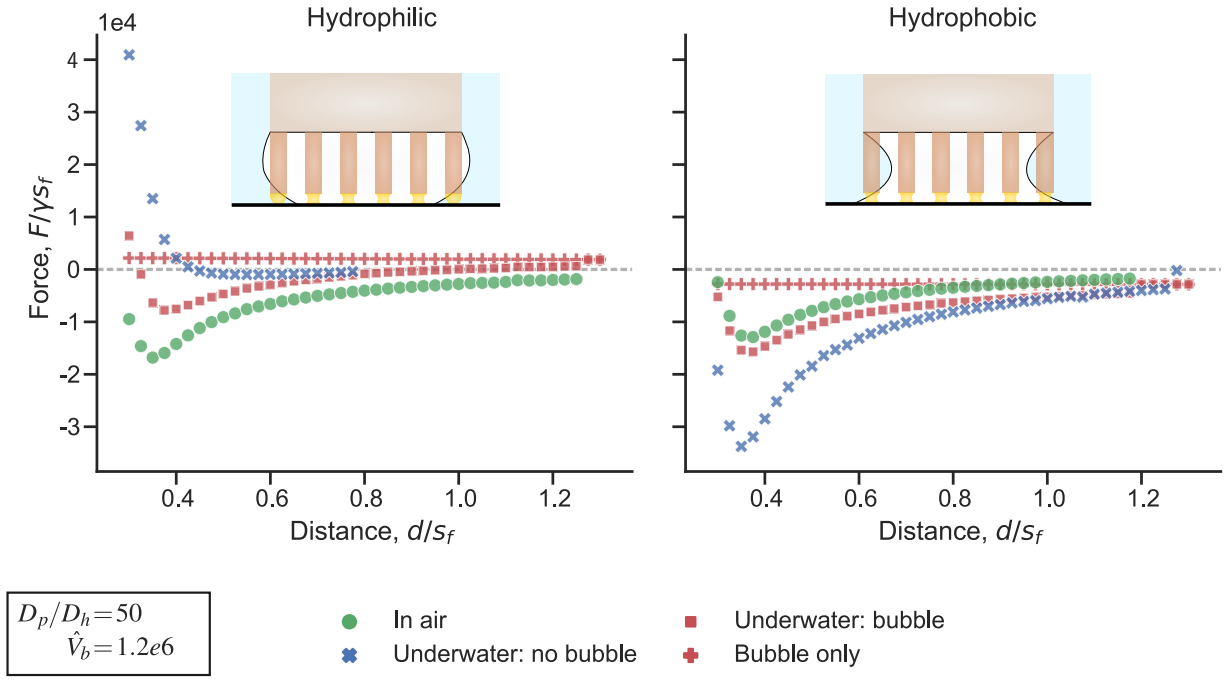

Figure 5: Theoretical force-distance curves of a hairy pad on a hydrophilic and hydrophobic substrate in air and underwater conditions. A negative force value represents attraction. Normalised forces are calculated from the capillary bridge model, with model parameters listed in Table 2. The bubble's contribution to the net force for an *underwater: bubble* contact is denoted by plus symbols. Insets represent the *underwater: bubble* contact for each substrate.

The observed trend in forces can be explained by how the tarsal adhesive fluid wets the surface in each case. On a hydrophilic substrate, the contact angle of the oily fluid is 6°, when surrounded by air (Table 2) and 150°, when surrounded by water (equation (3)). This results in the meniscus shape to have a net negative and slightly positive curvatures, respectively, resulting in strong adhesion in air and poor adhesion underwater. On a hydrophobic

substrate however, the contact angles of the fluid in air and water are 50° and 1°, respectively. In both cases, the contact angles are low, resulting in strong adhesion in both media. Additionally, the interfacial tension of the oily fluid underwater (γ_{fw}) is twice that of in air (γ_{fa}). Thus, we see a higher capillary adhesion for the *underwater: no bubble* case when compared to *in air* (Figure 6). Note that the contact area is fixed in all cases by keeping the area fraction and D_p/D_h constant. Thus the observed effects is not a result of changing contact area, but rather on the nature of capillary forces.

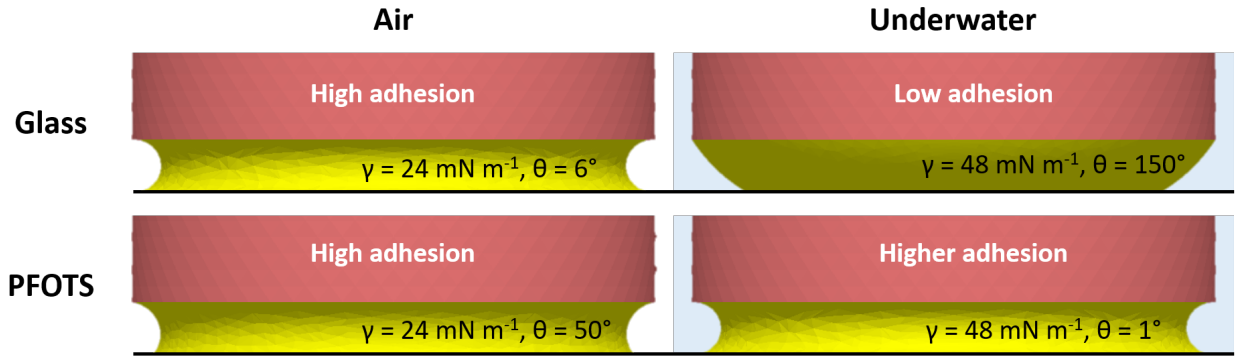

Figure 6: Simulation snapshots of oil capillary meniscus in contact with normal glass and PFOTS-coated glass in air and underwater conditions. The corresponding interfacial tension, γ, and contact angle, θ, used to predict the ladybug's adhesion are labelled for each case.

The net force in the *underwater: bubble* case mainly depends on the proportion of hairs inside and outside the bubble (equation (2)). For the given bubble volume, only part of the hairs make contact with the surface inside the bubble for the hydrophilic case, while, all the hairs contact the surface inside the bubble for the hydrophobic case. Therefore, the force curve lies between *in air* and *underwater: no bubble* cases for a hydrophilic substrate, and closely follows the *in air* case for a hydrophobic substrate.

We observed that the bubble itself doesn't contribute much to the net force on either substrate (Figure 5). Its contribution even is slightly repulsive on the hydrophilic substrate due to the positive curvature of the bubble, and slightly attractive on the hydrophobic substrate due to its negative curvature. This small contribution is manifested by the slightly higher adhesion for *underwater: bubble* relative to *in air* for the hydrophobic substrate, since

all hairs are within the bubble in this case.

3.4 Adhesion of a hairy pad: Effect of the air bubble volume

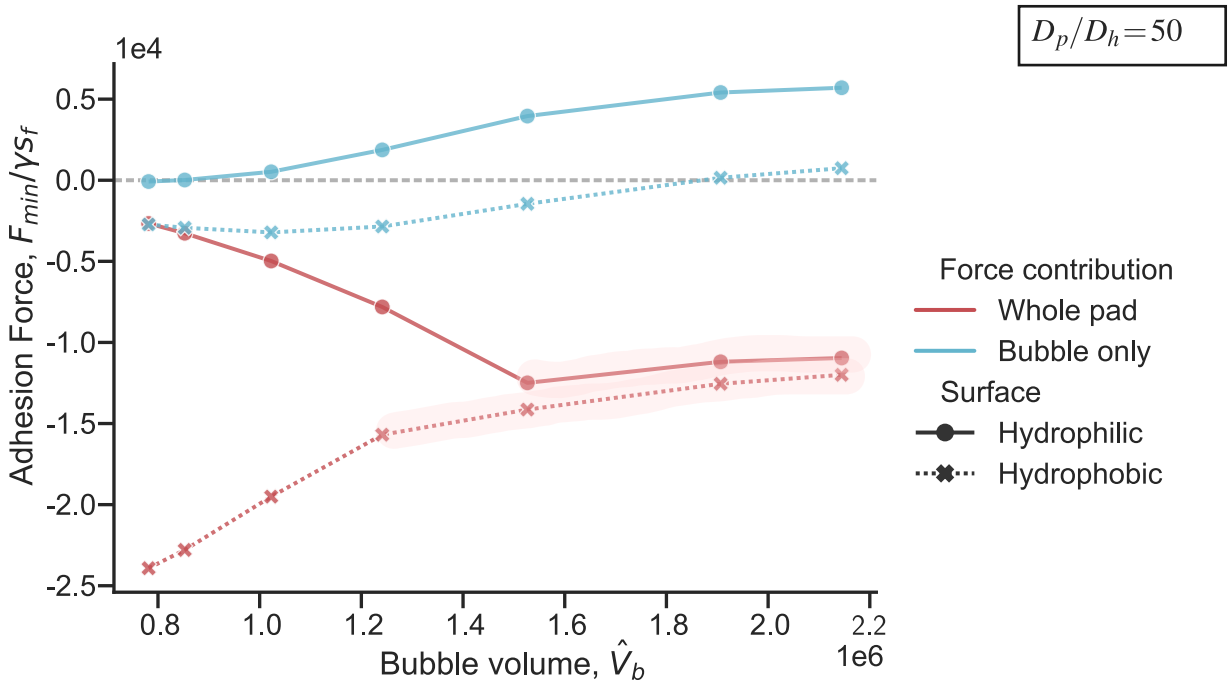

Figure 7: Normalised adhesion force of a hairy pad as a function of bubble volume, $\hat{V}_b$, for the *underwater: bubble* contact mode. Adhesion forces are calculated from the minima of the respective force-distance curves. Negative force value represents attraction. Pad to hair diameter ratio (D_p/D_h) is kept fixed. Highlighted regions represent entrapment of all hairs within the bubble.

The volume of the trapped air bubble can influence its capillary force contribution, as well as change the relative proportion of hairs inside and outside it. To investigate this, we varied the bubble volume, $\hat{V}_b$, and compared the maximum adhesion force on both hydrophilic and hydrophobic substrates (Figure 7). The contribution of the bubble to the net adhesion force is small regardless of its volume, when compared to the whole pad. Further, opposite trends of adhesion is seen on the two substrates with changing $\hat{V}_b$.

From the previous section, we know that on the hydrophilic substrate, fluid bridges outside the bubble show poor adhesion due to the positive curvature of their meniscus.

Thus, decreasing $\hat{V}_b$ decreases the adhesion force due to a larger proportion of tarsal hairs being outside the bubble. In contrast, on the hydrophobic substrate, fluid bridges outside the bubble showed higher capillary forces, due to its low contact angle and high interfacial tension in water. Thus, adhesion force increases for a hydrophobic substrate as the bubble size decreases.

A smaller $\hat{V}_b$ resulted in increased, but small, attraction by the bubble on both types of substrates. For larger values of $\hat{V}_b$ however, the force trend for the whole pad mostly follows that of the bubble. This is because the bubble gets big enough to entrap all the hairs inside it. Thus, the force contribution due to the fluid bridges remain unchanged, and only the bubble's contribution drives the slight variation in the pad's adhesion at high $\hat{V}_b$. Once the bubble is small enough such that part of the fluid bridges start making contact in water, the force trend changes, with a steep decrease (increase) in adhesion force on hydrophilic (hydrophobic) substrate as the volume decreases.

3.5 Adhesion of a hairy pad: Effect of the hair tip diameter

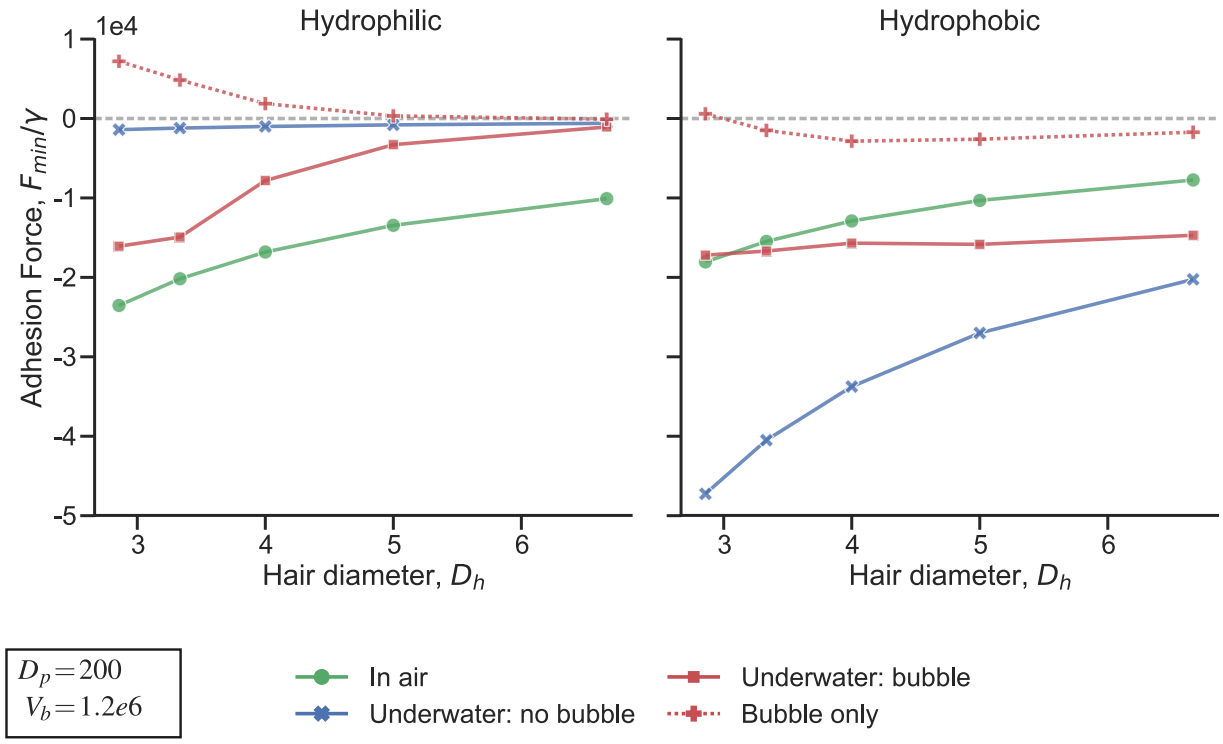

Figure 8: Normalised adhesion force of a hairy pad on a hydrophilic and hydrophobic substrate as a function of hair tip diameter, D_h. Volume of each fluid bridge, V_f, scales relative to D_h based on the parameter $\phi_f = 2$. Adhesion forces are calculated from the minima of the respective force-distance curves, based on the capillary bridge model. A negative value represents attraction. The air bubble's contribution to the net force for an *underwater: bubble* contact is denoted by plus symbols. Pad diameter and bubble volume are kept fixed. All lengths are scaled relative to D_p.

The tarsal hairs on a ladybug's adhesive pad terminate in various shapes, such as "discoidal" or "pointed". We studied this geometric effect on adhesion by changing the hair tip diameter, D_h (Figure 8). Here, the pad diameter, total hair contact area and bubble volume are constant since D_p, α and $\hat{V}_b$ are kept fixed. The tarsal adhesive fluid volume is again assumed to scale relative to the hair diameter ($\phi_f = 2$).

Adhesion force increases with decreasing D_h for both hydrophilic and hydrophobic substrates in all contact modes. This is consistent with the "contact splitting" theory, which predicts higher adhesion when the contact is split into many small contact points[24]. Re-

ducing the hair diameter results in two competing effects: 1) capillary force due to a single fluid bridge decreases due to its smaller size and "self-similar" scaling assumption ($f \sim D_h$), which decreases the net force, and 2) total number of fluid bridges increases since the total hair contact area is assumed to be fixed ($N \sim 1/D_h^2$), which increases the net force. The second effect dominates, resulting in a higher adhesion force as D_h decreases.

Similar to the trend in Figure 5, contact *in air* shows the highest adhesion force on a hydrophilic substrate for the given range of hair diameters, while on a hydrophobic substrate, *underwater: no bubble* shows highest adhesion. *Underwater: bubble* contact shows intermediate adhesion between *in air* and *underwater: no bubble* contact modes.

The bubble's contribution gets repulsive as hair diameter decreases for both substrates (Figure 8). Since the aspect ratio L/D_h is fixed (Table 2), decreasing the hair diameter also decreases its length. Since the bubble's volume is kept constant, it will then have a lesser space available to occupy between the pad and the substrate. This results in it bulging outwards near the pinned contact line on the top, causing repulsion.

4 Discussion

Our experiments demonstrate that the ladybug beetle can attach underwater to a hydrophobic substrate even without a bubble trapped around its tarsal hairs. A previous study[16] proposed that an air bubble is necessary for underwater attachment in terrestrial beetles. This is, however, only true for hydrophilic substrates, where a trapped air bubble can facilitate underwater adhesion due to the hairs making contact in a de-wetted environment. For a hydrophobic substrate, the adhesion is similar regardless of whether the contact occurs in air or underwater conditions, with or without a trapped bubble. Our theoretical calculations further show that the bubble by itself has a negligible capillary contribution to the net underwater adhesion of the pad. Direct force measurement of a single similarly sized bubble making contact with a hydrophobic substrate shows a maximum adhesion less than 50 µN,

which further validates that the bubble's contribution is insignificant (Figure S1.3).

Predictions of the ladybug's adhesion from the capillary bridge model agree with our experimental results (Figure 2). In underwater conditions without a trapped air bubble, adhesion to a hydrophobic substrate is significantly larger than to a hydrophilic substrate. This is explained by the different interfacial tension of the oily tarsal secretion and its contact angles with the substrates in air and underwater, which determines the capillary adhesive force in each case (Figure 6). However, the experiments don't show the predicted ~ 2.6 times increase in underwater adhesion relative to that in air on the hydrophobic PFOTS-coated surface. This discrepancy could be due to our assumptions of the oily fluid's interfacial properties. If we choose γ_{fa}=30 mN m^{-1} and γ_{fw}=40 mN m^{-1}, the corresponding increase in adhesion will be ~ 1.7, closer to our experimental value of ~ 1. The resulting change in θ_{fa} and θ_{fw} will further decrease this number. Direct measurement of the fluid's interfacial properties is thus essential to better predict the insect's adhesion, and will be a subject of future studies. Further, due to surface inhomogeneities, not all the hairs might be able to completely drain the interfacial water layer, in order for the tarsal adhesive fluid to make a direct contact with the substrate. This can further reduce underwater adhesion, in comparison to our theoretical predictions which assumes a perfect contact of all hairs' terminals.

In the model, we assume that all the hairs detach simultaneously to give a theoretical maximum achievable adhesion force. In our experiments, however, not all hairs make a perfect contact with the substrate despite our best efforts to align the pad parallel to the surface. Furthermore, during detachment, the constrained pad typically peels off from its proximal to distal end rather than detach simultaneously. Our model also assumes the hairs to be of similar geometry, unlike the male beetle's pad which has a distribution of flat or pointed tipped hairs. Thus, it's not surprising that the model overestimates the adhesion forces. The predictions are however in the same order of magnitude as experiments, and the qualitative trend is consistent for both hydrophilic and hydrophobic substrates in air and

underwater.

Our study provides further validation that capillary forces govern the ladybug's adhesion and van der Waals contribution, if any, must be negligible. Further, the capillary forces can even enable ladybug attachment underwater depending on the substrate chemistry. When underwater, without a trapped bubble, the pads adhere strongly to a hydrophobic substrate, but poorly to a hydrophilic substrate, even though it shows similarly strong adhesion to both substrates in air. This effect can be explained by capillary forces and the wetting properties of the fluid. Our preliminary chemical composition analysis of a beetle's tarsal secretions before and after immersing its leg underwater validates our assumption that the tarsal adhesive fluid should form capillary bridges with the substrate underwater, instead of getting washed away (see supplementary info Section S1.5).

To some extent, the findings could be extended to other animals relying on oily secretions for adhesion. For example, ants are known to possess smooth adhesive pads which secrete a fluid containing oily substances[9]. It has been reported that some ants show similar adhesion on hydrophobic substrates under wet and dry conditions[25], similar to what we see in a ladybug. This observation can again be explained by a capillary model as before. Recent experiments on geckos revealed that they can attach well to fluoropolymer substrates (such as PTFE) underwater while they show little adhesion to the same substrate in air[26,27]. Geckos are thought to rely on van der Waals forces via dry contact with the substrate[12], although recent observations of phospholipid footprints left behind walking geckos[28] could change that picture. Since geckos adhere poorly to PTFE (surface energy $\sim$ 20 mN m^{-1}) one can speculate that the phospholipid material has a higher surface energy, and consequently makes a higher contact angle with PTFE in air. Let us assume the phosopholipid substance to be a fluid similar to oil with γ_{fa}= 30 mN m^{-1} and γ_{fw}= 42 mN m^{-1} such that its contact angle with PTFE is 80°. Equation 3 then gives us an underwater contact angle of 70° for the phospholipid fluid. Thus, on a PTFE surface, the capillary bridge model can predict a higher adhesion underwater than in air due to its lower contact angle and higher interfacial energy

underwater. Based on similar assumptions, we predict the net adhesion force for the gecko on different substrates (Figure 9). The adhesion force predictions are in good qualitative agreement with the whole animal experimental shear force values reported for the gecko, with the trend of higher adhesion in air than underwater for glass, similar adhesion in air and underwater for PMMA/OTS-SAM and lower adhesion in air than underwater for PTFE. We, thus, propose that the underwater experiments performed on geckos[26,27] indicate a capillary contribution to gecko adhesion. Previous studies on gecko adhesion have attributed capillary effects to be a result of water condensation from ambient humid air onto the setal hair tips[29–31]. We however emphasize that capillary contribution in gecko adhesion could rather be a result of its setal phospholipid layer rather than water. The previously reported influence of humidity on gecko adhesion[29] could possibly be an effect of change in surface tension of the oily phospholipid layer at different humidity, which will in-turn influence the capillary adhesion force. We suggest performing single seta adhesion force tests similar to Autumn et al.[12] using a hydrophilic and fluorinated probe in air and underwater conditions. If the fluorinated probe shows higher adhesion underwater than in air on a single seta, this would confirm the role of capillary contributions due to an oil-like phospholipid layer to gecko adhesion. Further work is also necessary to validate if the phospholipid layer in geckos' toes indeed has fluid-like properties.

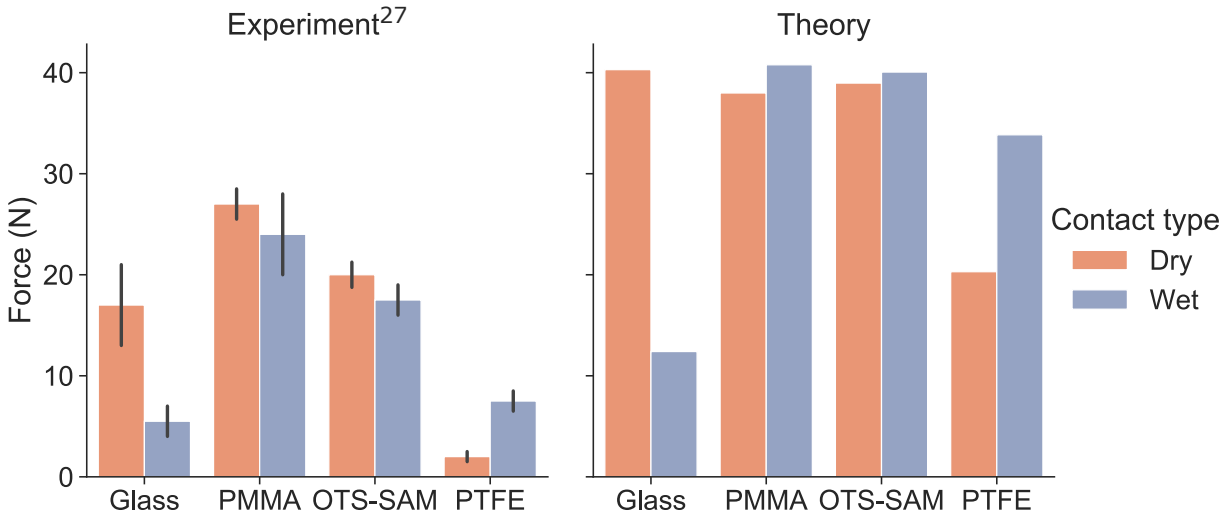

Figure 9: Whole animal adhesion force of geckos on various substrates. Experimental shear adhesion values are reproduced from Stark et al.[27]. Normal adhesion forces for each gecko toe are theoretically estimated from the capillary bridge model, with hair diameter = 400 nm, toe diameter = 4 mm, phospholipid fluid volume = 4.19x10^{-3} fL and 10% hair coverage. "*Underwater: no bubble*" contact mode is assumed for the "Wet" case. Net adhesion force is calculated by assuming 5 toes on each leg and 4 legs in total on a gecko. Interfacial tension of the phospholipid layer (PL) in air and water are assumed to be 30 mN m^{-1} and 42 mN m^{-1} respectively. PL contact angles with glass, PMMA, OTS-SAM and PTFE are assumed to be 6°, 10°, 20° and 80° respectively. The corresponding water contact angles are 50°, 85°, 94° and 97° respectively, as reported in Stark et al.[27].

We have so far limited our analysis to only smooth substrates. Of course insects have to cope with all kinds of surfaces including rough ones. Previous studies[32] have shown that substrate roughness is a more dominant parameter than substrate chemistry in controlling ladybug beetle traction force. Future work will explore how roughness can impact the net capillary force also in wet and submerged conditions. We have limited our analysis only to normal adhesive forces, but insects like beetles in general rely on friction or shear forces during locomotion. Friction force usually correlates directly with the normal force, which is probably why previously reported shear adhesion forces of the dock beetle[16] follow a similar qualitative trend as our normal adhesion force measurements on the ladybug beetle in both air and underwater conditions. However, the details of the interplay between friction and normal adhesion forces in animals is an open question and is beyond the scope of this paper.

Our study can contribute to potential applications in the design of bio-inspired materials to achieve underwater adhesion via capillary bridges. Introduced bubbles can possibly be used to control underwater adhesion by changing the relative proportion of the arrays inside and outside the bubble. A suitable choice of an adhesion-mediating fluid can be made tailored to the substrate and environment of application to form capillary bridges with optimal adhesion performance in bio-inspired fibrillar adhesive systems.

5 Conclusions

Ladybug beetles rely primarily on their oily fluid secretion at the tarsal hair tips to adhere to surfaces in both air and underwater conditions. The beetles can attach underwater on a hydrophobic substrate even without a trapped air bubble within its hairy pad, although it loses this ability on a hydrophilic substrate. This is explained theoretically by the different contact angle and interfacial tension of the secreted fluid in air and underwater conditions. Further, the bubble itself has a negligible capillary contribution to the total force. The trapped bubble can promote adhesion only on a hydrophilic substrate by providing an air medium to the adhesive fluid bridges inside it. Oil wettability, thus, primarily controls the insect's adhesion in any given condition. Our study highlights how a fluid-mediated strategy can help achieve strong adhesion even underwater. A similar argument also explains previously reported underwater adhesion force measurements in geckos[27], which suggests the possibility of capillary contributions to gecko adhesion mediated by an oil-like phospholipid layer. Future studies should characterise the fluid secretion's interfacial properties with a particular substrate to better understand the fundamental nature of an animal's adhesion.

6 Acknowledgement

We are grateful to Eduard Arzt and Renè Hensel (Leibniz Institute for New Materials, Saarbrücken, Germany) for fruitful discussions. This work was supported by the *Deutsche*

Forschungsgemeinschaft (Grant number: PI 1351/2-1) and the *Max Planck Graduate Center* with the *Johannes Gutenberg-Universität Mainz* (MPGC).

References

(1) Hooke, R. *Micrographia, or, Some physiological descriptions of minute bodies made by magnifying glasses : with observations and inquiries thereupon*; The Royal Society, 1665.

(2) Stork, N. E. Experimental Analysis of Adhesion of *Chrysolina Polita* (Chrysomelidae: Coleoptera) on a Variety of Surfaces. *The Journal of Experimental Biology* **1980**, *88*, 91.

(3) Gorb, S. N.; Beutel, R. G. Evolution of locomotory attachment pads of hexapods. *Naturwissenschaften* **2001**, *88*, 530–534.

(4) Coddington, J. A.; Levi, H. W. Systematics and evolution of spiders (*Araneae*). *Annual Review of Ecology and Systematics* **1991**, *22*, 565–592.

(5) Williams, E.; Peterson, J. Convergent and alternative disigns in the digital adhesive pads of scincid lizards. *Science* **1982**, *215*, 1509–1511.

(6) Federle, W. Why are so many adhesive pads hairy? *J Exp Biol* **2006**, *209*, 2611–21.

(7) Bullock, J. M.; Federle, W. Division of labour and sex differences between fibrillar, tarsal adhesive pads in beetles: effective elastic modulus and attachment performance. *J Exp Biol* **2009**, *212*, 1876–88.

(8) Bullock, J. M.; Federle, W. Beetle adhesive hairs differ in stiffness and stickiness: in vivo adhesion measurements on individual setae. *Naturwissenschaften* **2011**, *98*, 381–7.

(9) Federle, W.; Riehle, M.; Curtis, A. S.; Full, R. J. An Integrative Study of Insect Adhesion: Mechanics and Wet Adhesion of Pretarsal Pads in Ants. *Integrative and Comparative Biology* **2002**, *42*, 1100–1106.

(10) Langer, M. G.; Ruppersberg, J. P.; Gorb, S. Adhesion forces measured at the level of a terminal plate of the fly's seta. *Proceedings of the Royal Society of London. Series B: Biological Sciences* **2004**, *271*, 2209–2215.

(11) Dirks, J. H. Physical principles of fluid-mediated insect attachment - Shouldn't insects slip? *Beilstein J Nanotechnol* **2014**, *5*, 1160–6.

(12) Autumn, K.; Sitti, M.; Liang, Y. A.; Peattie, A. M.; Hansen, W. R.; Sponberg, S.; Kenny, T. W.; Fearing, R.; Israelachvili, J. N.; Full, R. J. Evidence for van der Waals adhesion in gecko setae. *Proceedings of the National Academy of Sciences* **2002**, *99*, 12252.

(13) Chen, Y.; Shih, M.-C.; Wu, M.-H.; Yang, E.-C.; Chi, K.-J. Underwater attachment using hairs: the functioning of spatula and sucker setae from male diving beetles. *Journal of The Royal Society Interface* **2014**, *11*.

(14) Kang, V.; White, R. T.; Chen, S.; Federle, W. Extreme suction attachment performance from specialised insects living in mountain streams (Diptera: Blephariceridae). *bioRxiv* **2020**,

(15) Seymour, R. S.; Matthews, P. G. D. Physical gills in diving insects and spiders: theory and experiment. *Journal of Experimental Biology* **2013**, *216*, 164–170.

(16) Hosoda, N.; Gorb, S. N. Underwater locomotion in a terrestrial beetle: combination of surface de-wetting and capillary forces. *Proc Biol Sci* **2012**, *279*, 4236–42.

(17) Peisker, H.; Gorb, S. N. Evaporation dynamics of tarsal liquid footprints in flies (*Cal-*

liphora vicina) and beetles (*Coccinella septempunctata*). *The Journal of Experimental Biology* **2012**, *215*, 1266–1271.

(18) Geiselhardt, S. F.; Geiselhardt, S.; Peschke, K. Comparison of tarsal and cuticular chemistry in the leaf beetle *Gastrophysa viridula* (Coleoptera: Chrysomelidae) and an evaluation of solid-phase microextraction and solvent extraction techniques. *Chemoecology* **2009**, *19*, 185.

(19) Attygalle, A. B.; Aneshansley, D. J.; Meinwald, J.; Eisner, T. Defense by foot adhesion in a chrysomelid beetle (*Hemisphaerota cyanea*): characterization of the adhesive oil. *Zoology* **2000**, *103*, 1–6.

(20) Ishii, S. Adhesion of a Leaf Feeding Ladybird *Epilachna vigintioctomaculta* (Coleoptera : Coccinellidae) on a Vertically Smooth Surface. *Applied Entomology and Zoology* **1987**, *22*, 222–228.

(21) Heepe, L.; Petersen, D. S.; Tölle, L.; Wolff, J. O.; Gorb, S. N. Sexual dimorphism in the attachment ability of the ladybird beetle Coccinella septempunctata on soft substrates. *Applied Physics A* **2016**, *123*, 34.

(22) Brakke, K. A. The surface evolver. *Experiment. Math.* **1992**, *1*, 141–165.

(23) De Souza, E. J.; Brinkmann, M.; Mohrdieck, C.; Arzt, E. Enhancement of Capillary Forces by Multiple Liquid Bridges. *Langmuir* **2008**, *24*, 8813–8820.

(24) Arzt, E.; Gorb, S.; Spolenak, R. From micro to nano contacts in biological attachment devices. *Proc Natl Acad Sci U S A* **2003**, *100*, 10603–6.

(25) Stark, A. Y.; Yanoviak, S. P. Adhesion and running speed of a tropical arboreal ant (*Cephalotes atratus*) on wet substrates. *Royal Society open science* **2018**, *5*, 181540–181540.

(26) Stark, A. Y.; Dryden, D. M.; Olderman, J.; Peterson, K. A.; Niewiarowski, P. H.; French, R. H.; Dhinojwala, A. Adhesive interactions of geckos with wet and dry fluoropolymer substrates. *Journal of The Royal Society Interface* **2015**, *12*, 20150464.

(27) Stark, A. Y.; Badge, I.; Wucinich, N. A.; Sullivan, T. W.; Niewiarowski, P. H.; Dhinojwala, A. Surface wettability plays a significant role in gecko adhesion underwater. *Proc Natl Acad Sci U S A* **2013**, *110*, 6340–5.

(28) Hsu, P. Y.; Ge, L.; Li, X.; Stark, A. Y.; Wesdemiotis, C.; Niewiarowski, P. H.; Dhinojwala, A. Direct evidence of phospholipids in gecko footprints and spatula - substrate contact interface detected using surface-sensitive spectroscopy. *Journal of The Royal Society Interface* **2012**, *9*, 657–664.

(29) Huber, G.; Mantz, H.; Spolenak, R.; Mecke, K.; Jacobs, K.; Gorb, S. N.; Arzt, E. Evidence for capillarity contributions to gecko adhesion from single spatula nanomechanical measurements. *Proceedings of the National Academy of Sciences of the United States of America* **2005**, *102*, 16293–16296.

(30) Kim, T. W.; Bhushan, B. The adhesion model considering capillarity for gecko attachment system. *Journal of The Royal Society Interface* **2008**, *5*, 319–327.

(31) Mitchell, C. T.; Dayan, C. B.; Drotlef, D.-M.; Sitti, M.; Stark, A. Y. The effect of substrate wettability and modulus on gecko and gecko-inspired synthetic adhesion in variable temperature and humidity. *Scientific Reports* **2020**, *10*, 19748.

(32) England, M. W.; Sato, T.; Yagihashi, M.; Hozumi, A.; Gorb, S. N.; Gorb, E. V. Surface roughness rather than surface chemistry essentially affects insect adhesion. *Beilstein journal of nanotechnology* **2016**, *7*, 1471–1479.